ELSEVIER

The Journal of Heart and Lung Transplantation

http://www.jhltonline.org

ORIGINAL CLINICAL SCIENCE

Right ventricular dyssynchrony in idiopathic pulmonary arterial hypertension: Determinants and impact on pump function

Roberto Badagliacca, MD, PhD,[a] Roberto Poscia, MD, PhD,[a] Beatrice Pezzuto, MD,[a] Silvia Papa, MD,[a] Cristina Gambardella, MD,[a] Marco Francone, MD,[b] Mario Mezzapesa, MD,[a] Martina Nocioni, MD,[a] Alfred Nona, MD,[a] Riccardo Rosati, MD,[b] Susanna Sciomer, MD,[a] Francesco Fedele, MD, FESC,[a] and Carmine Dario Vizza, MD[a]

From the Departments of [a]Cardiovascular and Respiratory Science; and [b]Radiological Science, Sapienza University of Rome, Rome, Italy.

KEYWORDS:
pulmonary arterial hypertension;
right ventricular function;
right ventricular dyssynchrony;
echocardiography;
2D speckle-tracking echocardiography;
right ventricular wall stress

BACKGROUND: Right ventricular (RV) dyssynchrony has been described in pulmonary arterial hypertension (PAH), but no evidence is available on its morphologic determinants and its effect on systolic function. The aim of this study was to evaluate the morphologic determinants of RV dyssynchrony by echocardiographic and cardiac magnetic resonance imaging and its effect on systolic function.

METHODS: In 60 consecutive idiopathic PAH (IPAH) patients with narrow QRS, RV dyssynchrony was evaluated by 2D speckle-tracking echocardiography, calculating the standard deviation of the times to peak systolic strain for the four mid-basal RV segments (RV-SD4). Patients were grouped by the median value of RV-SD4 (19 milliseconds) and compared for RV remodeling and systolic function parameters, WHO class, pulmonary hemodynamics and 6-minute walk test (6MWT).

RESULTS: Despite similar pulmonary vascular resistance and mean pulmonary arterial pressure, patients with RV-SD4 at >19 milliseconds had advanced WHO class and worse 6MWT, RV hemodynamics, RV remodeling and systolic function parameters compared with patients at ≤ 19 milliseconds. The morphologic determinants of RV dyssynchrony resulted RV end-diastolic area, LV diastolic eccentricity index and RV mass volume ratio ($r = 0.69$, $r^2 = 0.47$, $p < 0.0001$). Finally, we found a significant inverse correlation between RV mid-basal segments post-systolic shortening time and cardiac index ($r = -0.64$, $r^2 = 0.41$, $p = 0.001$), accounting for the significant correlation between RV-SD4 and cardiac index ($r = 0.57$, $r^2 = 0.32$, $p = 0.003$).

CONCLUSIONS: In IPAH with narrow QRS, RV dyssynchrony is associated with RV dilation and eccentric hypertrophy pattern, suggesting a role of segmental wall stress heterogeneity as the major determinant of mechanical delay. Post-systolic shortening, as inefficient contraction, contributes to pump dysfunction.

J Heart Lung Transplant ■■■■;■:■■■–■■■

© 2014 International Society for Heart and Lung Transplantation. All rights reserved.

Reprint requests: Roberto Badagliacca, MD, PhD, Department of Cardiovascular and Respiratory Science, I School of Medicine, Sapienza University of Rome, Policlinico Umberto I, Viale del Policlinico, 155-00161 Rome, Italy.

E-mail address: roberto.badagliacca@uniroma1.it

Idiopathic pulmonary arterial hypertension (IPAH) is characterized by a progressive increase in pulmonary vascular resistance (PVR), leading to right ventricular

1053-2498/$ - see front matter © 2014 International Society for Heart and Lung Transplantation. All rights reserved.
http://dx.doi.org/10.1016/j.healun.2014.06.010

(RV) overload. Prognosis depends on the ability of the RV to maintain efficiency in face of increased after-load, underscoring the fundamental role of RV adaptation mechanisms to guarantee cardiac output.[1] Left ventricular dyssynchrony has been identified as a major prognostic factor in left side chronic heart failure due to systolic left ventricular dysfunction[2] and it has been targeted using a non-pharmacologic approach.[3] Recently, RV mechanical dyssynchrony has been described in pulmonary arterial hypertension (PAH),[4–7] but limited data are available regarding its effects on cardiac output, as a result of adaptive or maladaptive compensatory mechanisms. Moreover, the morphologic determinants associated with mechanical dyssynchrony have not yet been evaluated in the setting of severe increased pulmonary pressure. Thus, the aim of this study was to evaluate the morphologic determinants of RV dyssynchrony using a comprehensive echocardiographic and cardiac magnetic resonance (CMR) imaging method, and to assess its effect on systolic function and cardiac output.

Methods

Population and study protocol

The study population included consecutive therapy-naive patients with IPAH, World Health Organization (WHO) Functional Class II to IV status, and without severe tricuspid regurgitation or electrocardiographic signs of intraventricular conduction delay. We excluded patients with a QRS duration of $\geq$120 milliseconds, as this implies an electromechanical delay. QRS duration was measured on a digital electrocardiographic (ECG) tracing at a velocity of 20 mm/second to obtain a precise assessment. Patients were referred to our Pulmonary Hypertension Unit (Policlinico Umberto I, Sapienza University of Rome, Italy) from January 2011 to December 2012.

The diagnosis of PAH relied on right heart catheterization (RHC) showing pre-capillary pulmonary hypertension (mean pulmonary artery pressure [mPAP] $\geq$25 mm Hg, pulmonary wedge pressure [PWP] $\leq$15 mm Hg) and use of an algorithm that included respiratory function tests, perfusion lung scan, computed tomography scan and echocardiography to rule out secondary causes, in accordance with European guidelines.[8]

Baseline evaluation at the time of diagnosis included medical history, physical examination, a non-encouraged 6-minute walk test (6MWT), RHC and echocardiographic and CMR assessment.

All patients were included in the study protocol after informed consent. The protocol was approved by the institutional review board for human studies of the Policlinico Umberto I, Sapienza University of Rome (Protocol No. 42412).

Right heart catheterization

Hemodynamic evaluation was made with standard technique. Pressures were measured from the mid-chest position with a fluid-filled catheter and pressure transducer; the average values over three respiratory cycles were recorded. Cardiac output (CO) was measured by the thermodilution technique (American Edwards Laboratories, Santa Ana, CA). The value for pulmonary vascular resistance (PVR) was calculated with the formula: PVR = (mPAP – PWP) / CO.

Standard echocardiography

Baseline echocardiographic studies were performed with the patient in the left lateral decubitus position using commercially available equipment (Vivid S6; GE Medical Systems). All echocardiographic data were acquired within 24 hours from RHC.

Data acquisition was performed with a 3.5-MHz transducer at a depth of 16 cm in the standard parasternal and apical views. Standard M-mode, 2D and Doppler images were obtained during breath-hold and stored in cine-loop format from three consecutive beats. Measurements were performed in accordance with the guidelines of the American Society of Echocardiography.[9]

The following parameters and derived measures were considered in the analysis: right atrial area (RA area); RV end-diastolic area (RVEDA); RV end-systolic area (RVESA); RV fractional area change percent [RVFAC = (RVEDA – RVESA) / RVEDA × 100]; tricuspid annular plane systolic excursion (TAPSE); left ventricular systolic and diastolic eccentricity index (LV-EIs and LV-EId, respectively); and presence of pericardial effusion.

Pulsed waved tissue Doppler imaging (PW-TDI) was used to measure longitudinal myocardial tissue velocities. These velocities were obtained with the transducer in the apical 4-chamber view and the sampling volume (5 mm) positioned in the center of the basal RV free wall segment, parallel to the analyzed vector of regional motion. Sector width, gains and filters were adjusted to obtain the optimal tissue signal. Measurements included the isovolumic contraction velocity (S1), isovolumic acceleration (IVA) and peak systolic velocity (S2). All reported measurements represent averages derived from three consecutive cardiac cycles.

RV dyssynchrony assessment

RV dyssynchrony was assessed using 2D speckle-tracking echocardiography.

Acquisition

For speckle-tracking analysis, standard gray-scale 2-dimensional (2D) images, previously acquired in the 4-chamber apical view and digitally saved in cine-loop format, were analyzed. Three consecutive beats were recorded with a frame rate between 50 and 70 fps to allow for reliable analysis of the software (ECHOPAC workstation 7.0.1; GE Medical Systems). The RV endocardial border was manually traced and a fine-tuning of the region of interest was done to ensure that the segments were tracked appropriately. Finally, the software automatically divided the myocardium into six standard segments (basal, middle and apical for the RV free wall and the interventricular septum) and time–strain longitudinal curves were generated from each segment.

Analysis

Peak systolic strain amplitude and time intervals from QRS onset to peak systolic strain were calculated for all RV myocardial segments in the longitudinal direction. Time intervals were corrected for heart rate according to Bazett's formula.[10]

To assess the segmental characteristics of the RV, we initially adopted the six-segment RV model, but then shifted to a four-segment RV model, excluding apical segments from the analysis due to their high variability, even among normal subjects. This

ARTICLE IN PRESS

decision has been supported previously by software-related technical data.[11]

To quantify RV dyssynchrony, we calculated the standard deviation (SD) of the times to peak-systolic strain for the four mid-basal RV segments corrected for the R–R interval between two QRS complexes, according to Bazett's formula, and called RV-SD4.

To define intra- and interobserver variability, 2D speckle-tracking measurements were repeated for 20 randomly selected patients by the same observer (B.R.) 2 weeks later and also by a second independent observer (R.M.). The mean differences, SD and 95% limits of agreement for the two measurements of the same observer (B.R.) and for the measurement of both observers (B.R. and R.M.) were calculated using the Bland–Altman test. Intra-observer and interobserver limits of agreements (95% confidence interval) were 2.6 to 3.4 milliseconds and 3.7 to 4.3 milliseconds, respectively, which was considered acceptable for our clinical objective.

CMR acquisition protocol

CMR studies were performed with a 1.5-T unit (Avanto Siemens, Erlangen, Germany) using dedicated cardiac software, phased-array surface receiver coil and ECG triggering, within 1 week of RHC.

Biventricular masses and volumes were determined using a breath-hold steady-state free-precession cine CMR technique acquired on both horizontal long- and short-axis planes, completely encompassing both ventricles with a stack of contiguous slices.

All CMR studies were analyzed offline by consensus of two experienced observers (F.M. and C.I., with 10 and 11 years of experience, respectively), using a dedicated workstation with cardiac software (CMR 42; Circle Canada).

Cine CMR was used to quantify RV and LV volumes (using four-chamber stacks), ejection fraction (EF) and RV/LV mass. Contours of images were traced semi-automatically at end-diastole and end-systole from horizontal long-axis planes, matching measurements with short-axis images when necessary.

Papillary muscle and trabeculations were included in the cavity. In basal slices, particular care was taken to exclude the atrium from the contours.

Statistical analysis

Continuous data are expressed as mean ± standard deviation, and categorical data are expressed as counts and proportions. Unrelated two-group comparisons were done with unpaired 2-tailed *t*-tests for means if the data were normally distributed or with Wilcoxon's rank-sum tests if the data were not normally distributed. Chi-square or Fisher's exact tests were used to analyze the categorical data. Linear regression analysis was performed to assess the relations between RV-SD4 and RV systolic function parameters and expressed as Pearson's correlation coefficient.

Multivariate regression analysis was used to identify the morphologic variables associated with RV dyssynchrony. Each variable with a significant association ($p < 0.05$) in univariate analysis and additional variables that were not significant but had potential clinical importance were introduced into a forward, stepwise regression model.

All statistical analyses were performed using SPSS, version 20.0 (IBM, Armonk, NY). Statistical tests were 2-sided, with $p < 0.05$ considered statistically significant.

Results

The original population consisted of 82 IPAH patients, but 3 patients had a poor echocardiographic window, 5 had severe tricuspid regurgitation, and 14 had a QRS duration of ≥120 milliseconds, so the final population included 60 IPAH patients. Table 1 summarizes patients' characteristics.

Table 1 Demographic, Clinical, Hemodynamic and RV Imaging Characteristics of the Study Population

Age (y)	55 ± 13
Gender (M:F)	21:39
Weight (kg)	71 ± 17
Height (cm)	166 ± 9
WHO functional class	2.5 ± 0.6
6MWT (m)	450 ± 110
Hemodynamics	
mPAP (mm Hg)	49 ± 14
RAP (mm Hg)	7.6 ± 4
CI (liters/min/m^2)	2.7 ± 0.8
PWP (mm Hg)	9.7 ± 3
PVR (WU)	8.9 ± 4.5
Compliance (ml/mm Hg)	1.48 ± 0.76
Echocardiography	
RA area (cm^2)	29 ± 11
LV-EId	1.33 ± 0.28
LV-EIs	1.53 ± 0.62
RVEDA (cm^2)	25 ± 9
RVESA (cm^2)	16 ± 7
RVFAC (%)	37 ± 11
TAPSE (mm)	20 ± 3
Pericardial effusion	16 (26%)
pTDI S1 (cm/s)	8.9 ± 2.5
pTDI S2 (cm/s)	10.5 ± 2.6
pTDI S1 acceleration slope (m/s^2)	2.8 ± 0.7
Peak 2DS mid RVFW (%)	19 ± 7
Peak 2DS basal RVFW (%)	22 ± 6
RV-SD4 mid basal (ms)	26.6 ± 23.6
CMR imaging	
RVEDV (ml)	166 ± 55
RVESV (ml)	113 ± 51
RVEF (%)	34 ± 12
RV mass (g)	68 ± 30
RV M/V ratio	0.43 ± 0.18

6MWT, non-encouraged 6-minute walk test; CI, cardiac index; WHO, World Health Organization; LV-EId, left ventricular end-diastolic eccentricity index; LV-EIs, left ventricular end-systolic eccentricity index; mPAP, mean pulmonary arterial pressure; peak 2DS middle and peak 2DS basal RVFW, 2-dimensional strain of the mid and basal segment of the RVFW by speckle-tracking echocardiography; pTDI S1, pulsed tissue Doppler peak isovolumic velocity at the basal RVFW segment; pTDI S2, pulsed tissue Doppler peak systolic velocity at the basal RVFW segment; PVR, pulmonary vascular resistance; PWP, mean pulmonary wedge pressure; RAP, mean right atrial pressure; RA area, right atrium area; RV M/V ratio, right ventricular mass/volume ratio; RVEDA, right ventricular end-diastolic area; RVESA, right ventricular end-systolic area; RVEDV, right ventricular end-diastolic volume; RVESV, right ventricular end-systolic volume; RVFAC, right ventricular fractional area change; RVFW, right ventricular free wall; RVFW, 2-dimensional strain of the basal segment of the RVFW by speckle-tracking echocardiography; RV-SD4 mid-basal, standard deviation of the times to peak-systolic strain for the four mid-basal RV segments; TAPSE, tricupid anular plane systolic excursion.

Table 2 Comparison of Clinical, Hemodynamic and RV Imaging Characteristics of IPAH Patients Grouped by RV-SD4 Median Value (19 milliseconds)

	RV-SD4 >19 ms	RV-SD4 ≤19 ms	*p*-value
Age (years)	52 ± 14	57 ± 13	NS
WHO functional class	2.8 ± 0.6	2.2 ± 0.5	0.001
6MWT (m)	401 ± 110	485 ± 97	0.003
Hemodynamics			
mPAP (mm Hg)	52 ± 16	47 ± 11	NS
RAP (mm Hg)	9 ± 5	6 ± 3	0.005
CI (liters/min/m^2)	2.5 ± 0.7	2.8 ± 0.7	0.03
PWP (mm Hg)	10 ± 3	9 ± 4	NS
PVR (WU)	10 ± 5	8 ± 4	NS
Compliance (ml/mm Hg)	1.36 ± 0.75	1.57 ± 0.77	NS
Echocardiography			
RA area (cm^2)	34 ± 13	26 ± 8	0.004
LV-Eid	1.43 ± 0.36	1.25 ± 0.18	0.01
LV-EIs	1.79 ± 0.86	1.34 ± 0.26	0.005
RVEDA (cm^2)	28 ± 10	22 ± 8	0.02
RVESA (cm^2)	19 ± 8	14 ± 6	0.009
RVFAC (%)	34 ± 13	40 ± 9	0.03
TAPSE (mm)	20 ± 4	21 ± 3	NS
Pericardial effusion	9 (15%)	7 (12%)	NS
pTDI S1 (cm/s)	8.5 ± 2.3	9.5 ± 2.5	0.03
pTDI S2 (cm/s)	8.9 ± 2.3	11.4 ± 3.0	0.01
pTDI S1 acceleration slope (m/s^2)	2.5 ± 0.6	3 ± 0.7	0.005
peak 2DS mid RVFW (%)	17 ± 7	22 ± 6	0.008
peak 2DS basal RVFW (%)	20 ± 6	24 ± 6	0.03
RV mid PSS (ms)	−42.3 ± 57.8	12.9 ± 27.6	0.0001
RV basal PSS (ms)	−48.4 ± 50.0	6.2 ± 28.9	0.0001
RV mid PSS (%)	−10 ± 15	5 ± 11	0.0001
RV basal PSS (%)	−13 ± 14	3 ± 11	0.0001
RV mid shortening time (ms)	338 ± 66	307 ± 36	0.02
RV basal shortening time (ms)	345 ± 60	314 ± 36	0.01
CMR imaging			
RVEDV (ml)	191 ± 50	151 ± 45	0.002
RVESV (ml)	131 ± 52	100 ± 46	0.01
RVEF (%)	29 ± 12	38 ± 11	0.004
RV mass (g)	78 ± 23	74 ± 25	NS
RV M/V ratio	0.41 ± 0.08	0.52 ± 0.15	0.002

6MWT, non-encouraged 6-minute walk test; CI, cardiac index; LV-EId, left ventricular end-diastolic eccentricity index; LV-EIs, left ventricular end-systolic eccentricity index; mPAP, mean pulmonary arterial pressure; peak 2DS mid RVFW, 2-dimensional strain of the mid-segment of the RVFW by speckle-tracking echocardiography; peak 2DS basal RVFW, 2-dimensional strain of the basal segment of the RVFW by speckle-tracking echocardiography; pTDI S1, pulsed tissue Doppler peak isovolumic velocity at the basal RVFW segment; pTDI S2, pulsed tissue Doppler peak systolic velocity at the basal RVFW segment; PSS, post-systolic shortening; PVR, pulmonary vascular resistance; PWP, mean pulmonary wedge pressure; RA area, right atrium area; RAP, mean right atrial pressure; RV M/V ratio, right ventricular mass/volume ratio; RVEDA, right ventricular end-diastolic area; RVEDV, right ventricular end-diastolic volume; RVESA, right ventricular end-systolic area; RVESV, right ventricular end-systolic volume; RVFAC, right ventricular fractional area change; TAPSE, tricupid anular plane systolic excursion; RVFW, right ventricular free wall; WHO, World Health Organization.

The majority of patients were female, in WHO Class III, and with severe PAH and impaired effort capacity. In comparing the two groups of patients divided by the median value of RV-SD4 (19 milliseconds), we found no significant differences in demographic characteristics (Table 2). Figures 1 and 2 show the different 2D speckle-tracking echocardiographic patterns of the two groups of patients. Despite similar PVR and mPAP, patients with RV-SD4 of >19 milliseconds had a more advanced WHO functional class and a worse exercise tolerance, RAP and CI compared with those at ≤19 milliseconds. Patients with RV-SD4 >19 milliseconds had also poorer RV remodeling, based on echocardiographic and CMR imaging, compared with the other patients. Interestingly, the two groups of patients had similar RV mass, but significantly different RV dimensional parameters, with greater RVEDA as RV dyssynchrony increased ($r = 0.48$, $p = 0.01$, $B = 1.26$; $\beta = 2.62$). These changes accounted for a more concentric hypertrophy (higher RV M/V ratio) in patients with RV-SD4 ≤19 milliseconds compared with the other patients.

Morphologic determinants of RV dyssynchrony

Multivariate regression analysis was used to identify the morphologic variables associated with RV dyssynchrony.

ARTICLE IN PRESS

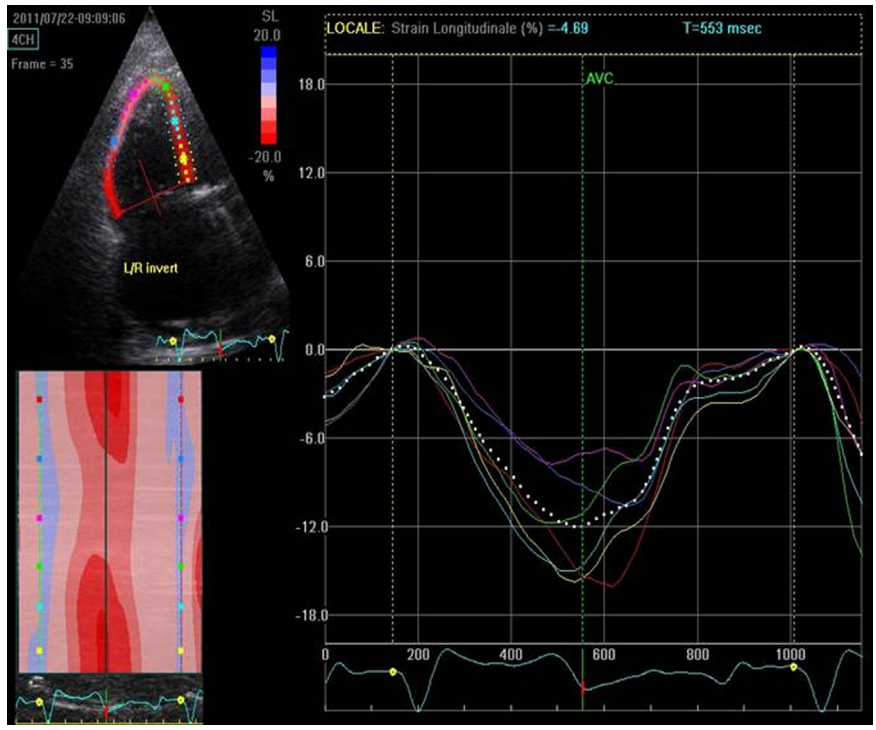

Figure 1 Tw-dimensional speckle-tracking imaging of longitudinal strain using the apical 4-chamber view to assess RV dyssynchrony—an example of a patient with RV-SD4 of 69 milliseconds. The segmental (colored lines) strain curves represent the relative (percentage) shortening of the six regions of interest as a function of time (in milliseconds). RV dyssynchrony by RV-SD4 is calculated as the standard deviation of the times from QRS onset (yellow dot in the QRS complex) to peak systolic strain for the four mid-basal RV segments corrected for the R–R interval between two QRS complexes (according to Bazett's formula).

Each variable with a significant association ($p < 0.05$) in the univariate analysis and additional variables that were not significant, yet had potential clinical importance, were introduced into a forward, stepwise regression model. Multivariate regression revealed that RVEDA, LV-EId and mass–volume (M/V) ratio were independent predictors of RV dyssynchrony ($r = 0.69$, $r^2 = 0.47$, $p < 0.0001$; Table 3). According to these results, patients with higher

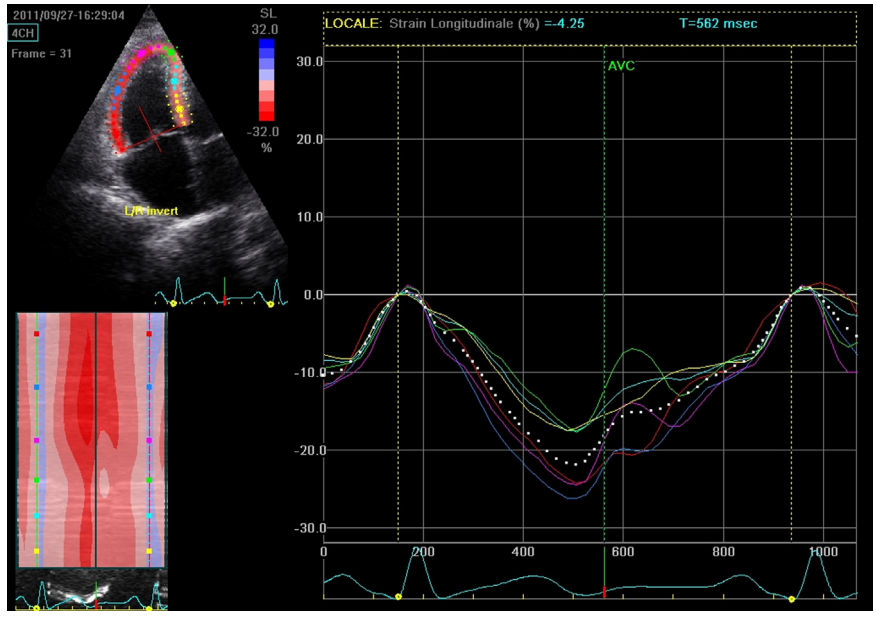

Figure 2 Two-dimensional speckle-tracking imaging of longitudinal strain using the apical 4-chamber view to assess RV dyssynchrony—an example of a patient with RV-SD4 of 9 milliseconds. The segmental (colored lines) strain curves represent the relative (percentage) shortening of the six regions of interest as a function of time (in milliseconds). RV dyssynchrony by RV-SD4 is calculated as the standard deviation of the times from QRS onset (yellow dot in the QRS complex) to peak systolic strain for the 4 mid-basal RV segments corrected for the R–R interval between two QRS complexes (according to Bazett's formula).

Table 3 Multivariate Analysis of RV Morphologic Variables Associated With RV Dyssynchrony[a]

	β	*B*	SE	*p*-value
Intercept		47.0	14.8	0.002
RVEDA	0.41	1.08	0.3	0.002
LV-EId	0.48	38.8	12.6	0.003
RV M/V ratio	−0.31	−52.5	17.2	0.001

B, unstandardized regression coefficient; β, standardized regression coefficient;
LV-EId, left ventricular end-diastolic eccentricity index; RV M/V ratio, right ventricular mass/volume ratio; RVEDA, right ventricular end-diastolic area.
[a] $R = 0.68$, $R^2 = 0.47$, adjusted $R^2 = 0.43$, $F = 11{,}74$, $p < 0.0001$. Standard error (SE) of estimate = 17.99.

RVEDA and LV-EId values are likely to have greater RV dyssynchrony, whereas those with a higher M/V ratio are more likely to have lower RV dyssynchrony.

RV dyssynchrony and systolic pump function

Patients with RV-SD4 >19 milliseconds had more impaired RV systolic function parameters, both by echocardiographic and CMR imaging evaluation, compared with the other patients, with the exception of TAPSE (19.7 mm vs 21.1 mm, respectively, p = not statistically significant [NS]; see Table 2). Patients in the former group also had a reduced CI and 6MWT distance compared with the latter group (2.5 liters/min/m^2 vs 2.9 liters/min/m^2, $p = 0.04$; and 401 ± 109 m vs 484 ± 97 m, $p = 0.003$, respectively).

On analysis of the relationship between CI and RV systolic function parameters among patients with RV-SD4 >19 milliseconds, the strongest inverse correlation was found with RV mid and basal segments post-systolic shortening ($r = -0.64$, $r^2 = 0.41$, $p = 0.001$; Figure 3),

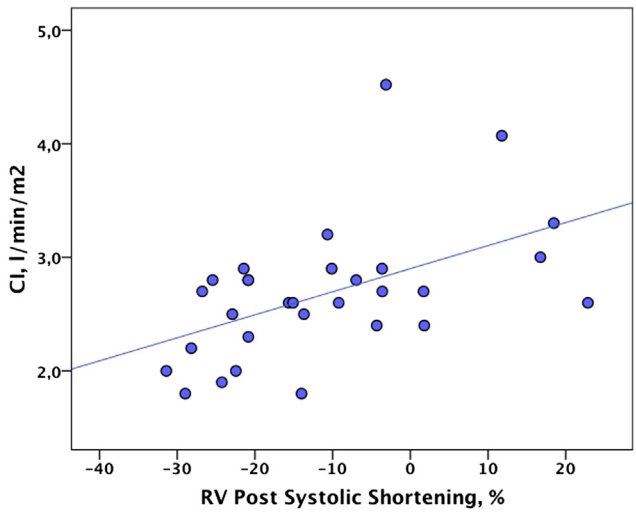

Figure 3 Scatterplots of cardiac index (CI) and post-systolic shortening. Correlation between CI and post-systolic shortening ($r = -0.64$, $r^2 = 0.41$, $p = 0.001$; $y = 3.1 + 0.008x$). Negative values of post-systolic shortening indicate percentage of RV free wall total systolic shortening time occurring after pulmonary valve closure.

the latter representing RV free wall systolic shortening time after pulmonary valve closure (Figure 4). This finding may account for the significant correlation found between RV-SD4 and CI ($r = 0.57$, $r^2 = 0.32$, $p = 0.003$). A weaker correlation was found between CI and RVFAC ($r = 0.33$, $p = 0.009$), RVEF ($r = 0.35$, $p = 0.006$), PW-TDI RV S2 ($r = 0.26$, $p = 0.04$) and peak 2DS mid-RVFW ($r = 0.37$, $p = 0.004$).

Discussion

In patients with left side chronic heart failure, left ventricular dyssynchrony is a well-established prognostic factor and a target for therapeutic intervention.[2,3] In this study we have evaluated the presence of RV dyssynchrony in one of the most severe forms of right side heart failure (i.e., IPAH) to assess its morphologic determinants and the impact on pump capacity.

Our results demonstrate that RV dyssynchrony is associated with RV dilation, interventricular septum diastolic flattening and eccentric hypertrophy (low RV mass / diastolic volume ratio). The other relevant finding is that RV dyssynchrony is inversely related to CI as it causes RV post-systolic shortening with inefficient contraction occurring after pulmonary valve closure.

RV dyssynchrony and chamber remodeling

Our findings show that RV dilation and a pattern of eccentric hypertrophy, with a disproportionate increase in ventricular volume compared with mass, are related to RV dyssynchrony.

These data are in apparent contrast with those from a recent study[7] that assessed a mixed pediatric population of PAH patients (mainly IPAH and PAH due to congenital heart disease). In that study the investigators found a high prevalence of RV dyssynchrony, but no correlation with any morphologic parameters of the RV. This is unsurprising because their study cohort included a large proportion of patients with a wide QRS, in which dyssynchrony was mainly related to electrical activation delay. This phenomenon could be related to the changes seen in animal models of PH in which RV overload caused conduction abnormalities through a modification of electrophysiologic cell properties and cell-to-cell coupling.[12,13] In our study, no patients had a wide QRS, and therefore this mechanism seems unlikely.

Regarding the morphologic determinants of RV dyssynchrony, one possible explanation is the role of non-uniform distribution of wall stress within the RV.

According to Laplace's law, wall stress is proportional to intraventricular pressure and cavity radius, and it is inversely related to wall thickness. As the RV shape is complex (i.e., the cavity radius changes for the different curvatures of each segment) and the wall thickness is not uniform through the ventricle, wall stress is heterogeneous, even in the normal right ventricle. The non-uniformity of wall stress is amplified in PAH as a consequence of the high

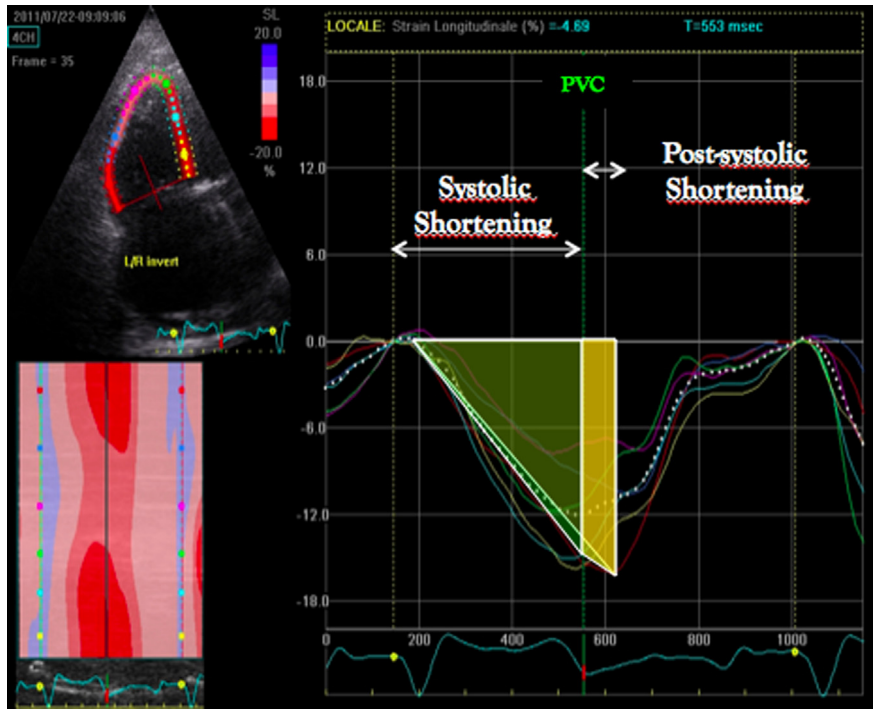

Figure 4 Two-dimensional speckle-tracking imaging of longitudinal strain using the apical 4-chamber view, illustrating post-systolic shortening of the RV basal segment (red line) in a patient with RV dyssynchrony (RV-SD4 69 milliseconds). The segmental (colored lines) strain curves represent the relative (percentage) shortening of the six regions of interest as a function of time (milliseconds). The green area represents systolic shortening of the RV basal segment, whereas the yellow area represents inefficient post-systolic shortening occurring after pulmonary valve closure. PVC, pulmonary valve closure (green dot vertical line).

intraventricular pressure and the type of RV remodeling pattern.[14] This means that, for the same level of intraventricular pressure, patients with RV eccentric hypertrophy (i.e., thinner wall or lower mass and larger radius or diastolic volume) have greater global and regional wall stress than patients with RV concentric hypertrophy.[15,16] Moreover, in eccentric hypertrophy remodeling, the increased RV diastolic volume and LV underfilling[17,18] cause interventricular septum dislocation toward the LV (LV-EId), the other determinant of RV dyssynchrony, with a significant distortion of RV chamber geometry.

In this setting, the non-uniform distribution of regional RV wall stress could contribute to mechanical dyssynchrony by a mere heterogeneity of contractile strength within the ventricle. Thus, an area with a lower regional stress (more hypertrophy and/or shorter radius from the geometrical center of the ventricle) will have different timing in peak strain than an area with higher regional stress.[19] In this case, the use of electrical resynchronization would probably be ineffective, as dyssynchrony is not related to electrical activation delay.

RV dyssynchrony and pump function

Among the overall IPAH population, patients with higher RV dyssynchrony showed a more advanced WHO functional class and worse exercise tolerance, as expressed by the 6MWT distance. These results are in accordance with the greater impairment of RV systolic function seen in these patients, despite similar mPAP, PVR and RV mass. These findings may be explained by a more unfavorable RV phenotype in patients with higher RV dyssynchrony, in whom the pattern of eccentric hypertrophy (lower mass/volume ratio) causes increased wall stress.

Previous studies in animal and human models have demonstrated that increased RV wall stress in PH may have several contractile consequences, showing a maladaptive switch from the α- to β-isotype of the myosin heavy chain, with lower adenosine triphosphatase activity, and abnormal contractile regulatory proteins expression in cardiomyocytes.[20–23] These pathophysiologic consequences together with RV myocardial ischemia[24-25] and increased cardiomyocyte apoptotic rates,[26–28] both described in chronically increased RV wall stress, may ultimately affect RV contractile performance and thus the systolic function parameters. Unexpectedly, among all RV systolic function parameters, TAPSE was the only one to show no significant difference between the two groups of patients. A possible explanation is the influence on tricuspid plane motion by the translation of overall cardiac motion. This phenomenon may cause an overestimation of TAPSE, particularly in patients with advanced RV remodeling, as seen in those with higher RV dyssynchrony, where the rocking motion of the heart is more evident.[29]

Finally, another major mechanism of RV pump dysfunction directly related to dyssynchrony was found to be post-systolic shortening time. Indeed, our findings show that RV dyssynchrony is correlated with CI, in accordance with previous data obtained using magnetic resonance analysis.[6]

In that study, Marcus et al suggested that dyssynchrony may reduce stroke volume by inefficient RV shortening occurring after pulmonary valve closure (i.e., post-systolic shortening; Figure 4). Our findings demonstrate, for the first time, that post-systolic shortening time is significantly negatively correlated with CI, accounting for 41% of the phenomenon (Figure 3).

Study limitations

Our study cohort consisted of patients referred to a single tertiary center, which may constitute a referral bias. However, this is a common limitation of similar studies. The second limitation is that the duration of disease may have influenced the development of RV dyssynchrony. However, determining the onset and duration of disease in PAH is challenging. We were thus unable to evaluate its influence on RV dyssynchrony. A possible technical limitation comes from use of 2D speckle-tracking echocardiography analysis, which requires experience to achieve high-quality results. However, as a rare disease, PAH management is mainly restricted to referral centers where expertise in echocardiographic evaluation is the standard of care. Finally, this study was cross-sectional and thus cause–effect relationships could not be established.

In conclusion, this study is the first to evaluate RV dyssynchrony by taking into account all morphologic and functional RV chamber features using a comprehensive echocardiographic and CMR imaging approach. Our findings suggest that, in patients with narrow QRS, RV dyssynchrony is:

(a) Associated with more advanced RV chamber remodeling.
(b) Likely due to the increased RV wall stress and its non-uniform distribution.
(c) A possible contributor to reduced cardiac output, through post-systolic shortening.

More studies are needed regarding whether RV dyssynchrony has an impact on survival in PAH and whether PAH-specific therapies may reverse RV dyssynchrony by reducing after-load and modifying RV chamber geometry. There is also a need to clarify the role of RV resynchronization in patients with significant electromechanical delay.

Disclosure statement

The authors have no conflicts of interest to disclose. Manuela Reali and Iacopo Carbone assisted as secondary observers in the echocardiographic and magnetic resonance imaging evaluations, respectively.

References

1. Voelkel NF, Quaife RA, Leinwand LA, et al. Right ventricular function and failure: report of a National Heart, Lung, and Blood Institute working group on cellular and molecular mechanisms of right heart failure. Circulation 2006;114:1883-91.
2. Bader H, Garrigue S, Lafitte S, et al. Intra-left ventricular electromechanical asynchrony. A new independent predictor of severe cardiac events in heart failure patients. J Am Coll Cardiol 2004;43:248-56.
3. Cleland JG, Daubert JC, Erdmann E, et al. The effect of cardiac resynchronization on morbidity and mortality in heart failure. N Engl J Med 2005;352:1539-49.
4. Lopez-Candales A, Dohi K, Bazaz R, et al. Relation of right ventricular free wall mechanical delay to right ventricular dysfunction as determined by tissue Doppler imaging. Am J Cardiol 2005;96:602-6.
5. Kalogeropoulos AP, Georgiopoulou VV, Howell S, et al. Evaluation of right intraventricular dyssynchrony by two-dimensional strain echocardiography in patients with pulmonary arterial hypertension. J Am Soc Echocardiogr 2008;21:1028-34.
6. Marcus JT, Gan CT, Zwanenburg JJM, et al. Interventricular mechanical asynchrony in pulmonary arterial hypertension: left-to-right delay in peak shortening is related to right ventricular overload and left ventricular underfilling. J Am Coll Cardiol 2008;51:750-7.
7. Hill AC, Maxey DM, Rosenthal DN, et al. Electrical and mechanical dyssynchrony in pediatric pulmonary hypertension. J Heart Lung Transplant 2012;31:825-30.
8. Galiè N, Hoeper MM, Humbert M, et al. ESC Committee for Practice Guidelines (CPG). Guidelines for the diagnosis and treatment of pulmonary hypertension: the Task Force for the Diagnosis and Treatment of Pulmonary Hypertension of the European Society of Cardiology (ESC) and the European Respiratory Society (ERS), endorsed by the International Society of Heart and Lung Transplantation (ISHLT). Eur Heart J 2009;30:2493-537.
9. Rudski LG, Lai WW, Afilalo J, et al. Guidelines for the echocardiographic assessment of the right heart in adults: a report from the American Society of Echocardiography. Endorsed by the European Association of Echocardiography, a registered branch of the European Society of Cardiology, and the Canadian Society of Echocardiography. J Am Soc Echocardiogr 2010;23:685-713.
10. Bazett HC. An analysis of the time-relations of electrocardiograms. Heart 1920;7:353-70.
11. NTNU-Trondhein Norwegian University of Science and Technology strain rate imaging. www.ntnu.edu/isb/echocardiography.
12. Zhu WX, Johnson SB, Brandt R, et al. Impact of volume loading and load reduction on ventricular refractoriness and conduction properties in canine congestive heart failure. J Am Coll Cardiol 1997;30:825-33.
13. Lee JK, Kodama I, Honjo H, et al. Stage-dependent changes in membrane currents in rats with monocrotaline-induced right ventricular hypertrophy. Am J Physiol 1997;272:H2833-42.
14. Simon MA, Deible C, Mathier MA, et al. Phenotyping the right ventricle in patients with pulmonary hypertension. Clin Transl Sci 2009;2:294-9.
15. Norton JM. Toward consistent definitions for preload and afterload. Adv Physiol Educ 2001;25:53-61.
16. Ryan T, Petrovic O, Dillon JC, et al. An echocardiographic index for separation of right ventricular volume and pressure overload. J Am Coll Cardiol 1985;5:918-24.
17. Mauritz GJ, Kind T, Marcus JT, et al. Progressive changes in right ventricular geometric shortening and long-term survival in pulmonary arterial hypertension. Chest 2012;141:935-43.
18. Hinderliter AL, Willis PW, Barst RJ, et al. Effects of long-term infusion of prostacyclin (epoprostenol) on echocardiographic measures of right ventricular structure and function in primary pulmonary hypertension. Circulation 1997;95:1479-86.
19. Kass DA. An epidemic of dyssynchrony. J Am Coll Cardiol 2008;51:12-7.
20. Lowes BD, Minobe W, Abraham WT, et al. Changes in gene expression in the intact human heart: downregulation of alpha-myosin heavy chain in hypertrophied, failing ventricular myocardium. J Clin Invest 1997;100:2315-24.
21. Herron TJ, McDonald KS. Small amounts of alpha-myosin heavy chain isoform expression significantly increase power output of rat cardiac myocyte fragments. Circ Res 2002;90:1150-2.

ARTICLE IN PRESS

22. Adamcova M, Sterba M, Simunek T, et al. Myocardial regulatory proteins and heart failure. Eur J Heart Fail 2006;8:333-42.
23. Bogaard HJ, Abe K, Vonk Noordegraaf A, et al. The right ventricle under pressure. Cellular and molecular mechanisms of right heart failure in pulmonary hypertension. Chest 2009;135:794-804.
24. van Wolferen SA, Marcus JT, Westerhof N, et al. Right coronary artery flow impairment in patients with pulmonary hypertension. Eur Heart J 2008;29:120-7.
25. Gomez A, Bialostozky D, Zajarias A, et al. Right ventricular ischemia in patients with primary pulmonary hypertension. J Am Coll Cardiol 2001;38:1137-42.
26. Hein S, Arnon E, Kostin S, et al. Progression from compensated hypertrophy to failure in the pressure-overloaded human heart: structural deterioration and compensatory mechanisms. Circulation 2003;107:984-91.
27. Olivetti G, Abbi R, Quaini F, et al. Apoptosis in the failing human heart. N Engl J Med 1997;336:1131-41.
28. Braun MU, Szalai P, Strasser RH, et al. Right ventricular hypertrophy and apoptosis after pulmonary artery banding: regulation of PKC isozymes. Cardiovasc Res 2003;59:658-67.
29. Giusca S, Dambrauskaite V, Scheurwegs C, et al. Deformation imaging describes right ventricular function better than longitudinal displacement of the tricuspid ring. Heart 2010;96:281-8.